

Radio Loud and Radio Quiet QSOs

K. I. Kellermann¹ and J. J. Condon¹

*National Radio Astronomy Observatory, 520 Edgemont Rd., Charlottesville, VA 22903,
USA*

kkellerm@nrao.edu

A. E. Kimball¹ and R. A. Perley¹

National Radio Astronomy Observatory, Socorro, NM 87801, USA

and

Željko Ivezić

*Department of Astronomy, University of Washington, Box 351580, Seattle, WA 98195,
USA*

ABSTRACT

We discuss 6 GHz JVLA observations covering a volume-limited sample of 178 low redshift ($0.2 < z < 0.3$) optically selected QSOs. Our 176 radio detections fall into two clear categories: (1) About 20% are radio-loud QSOs (RLQs) having spectral luminosities $L_6 \gtrsim 10^{23.2} \text{ W Hz}^{-1}$ primarily generated in the active galactic nucleus (AGN) responsible for the excess optical luminosity that defines a *bona fide* QSO. (2) The radio-quiet QSOs (RQQs) have $10^{21} \lesssim L_6 \lesssim 10^{23.2} \text{ W Hz}^{-1}$ and radio sizes $\lesssim 10 \text{ kpc}$, and we suggest that the bulk of their radio emission is powered by star formation in their host galaxies. “Radio silent” QSOs ($L_6 \lesssim 10^{21} \text{ W Hz}^{-1}$) are rare, so most RQQ host galaxies form stars faster than the Milky Way; they are not “red and dead” ellipticals. Earlier radio observations did not have the luminosity sensitivity $L_6 \lesssim 10^{21} \text{ W Hz}^{-1}$ needed to distinguish between such RLQs and RQQs. Strong, generally double-sided, radio emission spanning $\gg 10 \text{ kpc}$ was found associated with 13 of the 18 RLQ cores having peak flux densities $S_p > 5 \text{ mJy beam}^{-1}$ ($\log(L) \gtrsim 24$). The radio luminosity function of optically selected QSOs and the extended radio emission associated

¹The National Radio Astronomy Observatory is a facility of the National Science Foundation operated under cooperative agreement by Associated Universities, Inc.

with RLQs are both inconsistent with simple “unified” models that invoke relativistic beaming from randomly oriented QSOs to explain the difference between RLQs and RQQs. Some intrinsic property of the AGNs or their host galaxies must also determine whether or not a QSO appears radio loud.

Subject headings: galaxies: quasars:general

1. Introduction

Fifty years after the discovery of optically selected QSOs, the distinction between radio-loud QSOs (RLQs) and radio-quiet QSOs (RQQs) is still being debated. In a preliminary report, Kimball et al. (2011) discussed 6 GHz observations of an optically selected QSO sample taken from the SDSS. These observations, made with the Karl G. Jansky Very Large Array (VLA), achieved unprecedented sensitivity which led to the detection of 97% of the SDSS QSOs with $M_i < -23$ in a low-redshift ($0.2 < z < 0.3$) volume-limited sample. In this paper, we report the full results of these observations including a new data analysis that detects 99% of the 178 studied QSOs with $M_i < -23$ in a low-redshift ($0.2 < z < 0.3$) volume-limited sample. Section 2 reviews the different criteria used to distinguish RLQs from RQQs and the evidence that RLQs and RQQs are or are not distinct populations. In Section 3 we describe our volume-limited sample of low-redshift QSOs and present results from the VLA observations that suggests that for most QSOs, the low luminosity ($10^{21} \lesssim L_6 \lesssim 10^{23} \text{ W Hz}^{-1}$) radio emission is primarily the result of star formation in the host galaxy, while the emission in the more luminous objects the radio emission is related to the SMBH. Section 4 includes notes on individual sources. In Section 5 we discuss differences between RLQs and RQQs. Our conclusions are summarized in Section 6.

All calculations in this paper assume a flat Λ CDM cosmology with $H_0 = 70 \text{ km s}^{-1} \text{ Mpc}^{-1}$ and $\Omega_\Lambda = 0.7$. Spectral luminosities are specified by their source-frame frequencies, flux densities are specified in the observer’s frame, and a mean spectral index $\alpha \equiv d \log(S)/d \log(\nu) = -0.7$ is used to make frequency conversions (see Kimball et al. (2011) for details).

2. Background

Shortly following the recognition that quasi-stellar radio sources were surprisingly luminous at both radio and optical wavelengths (Schmidt 1963; Greenstein 1963; Greenstein & Schmidt 1964; Schmidt 1965), Allan Sandage (1965) announced “The Existence of a Major New

Constituent of the Universe: the Quasistellar Galaxies” which were optically selected and outnumbered the known (and extremely radio loud) quasi-stellar radio sources by a factor of $\sim 10^3$. Sandage’s dramatic announcement was published in the May 1, 1965 issue of the *Astrophysical Journal* (the same day that it was received at the journal office) and created considerable controversy. Zwicky (1965) immediately pointed out that he had previously reported on similar objects which he called “blue compact galaxies,” while Kinman (1965) and Lynds & Villere (1965) argued that most of Sandage’s claimed quasi-stellar galaxies are only blue stars in our Galaxy. Nevertheless, it is now widely recognized that Sandage’s quasi-stellar galaxies, today called quasi-stellar objects (QSOs), do outnumber quasi-stellar radio sources, albeit only by about an order of magnitude.

Although the term “quasar” is a portmanteau of “quasi-stellar radio source” (Chiu 1964), here we follow the definitions given by Schmidt (1970) and endorsed by the *Astrophysical Journal* that (1) quasars include all extragalactic objects of “starlike appearance (or containing a dominant starlike component),” even “buried” objects reddened or obscured by dust and objects selected at infrared or X-ray wavelengths, and (2) QSOs are quasars selected optically. Schmidt & Green (1983) quantified the requirement for a “dominant starlike component” to distinguish *bona fide* QSOs from less-luminous AGNs such as Seyfert nuclei: QSOs must have $M_B \leq -23$ when calculated using $H_0 = 50 \text{ km s}^{-1} \text{ Mpc}^{-1}$ and $q_0 = 0.1$. In the modern Λ CDM cosmology with $H_0 = 70 \text{ km s}^{-1} \text{ Mpc}^{-1}$, $\Omega_m = 0.3$, and $\Omega_\Lambda = 0.7$, such QSOs have absolute magnitudes $M_B \leq -22.2$. However, most authors still use $M_B < -23$, following the letter but not the spirit of the Schmidt & Green (1983) criterion, and we also use that $0.8 \text{ mag} \approx 2$ times more luminous limit for QSOs.

Early targeted searches for radio emission from QSOs (Kellermann & Pauliny-Toth 1966; Shapiro & Weinreb 1966; Katgert et al. 1973; Fanti et al. 1977; Smith & Wright 1980; Sramek & Weedman 1980; Condon et al. 1980a,b) had $\sim 10\%$ detection rates. Somewhat surprisingly, the radio detection rate grew very slowly as the flux-density limit was lowered, leading to the suggestion that radio-loud QSOs (RLQs) and radio-quiet QSOs (RQQs) might have different flux-density distributions and thus comprise two distinct populations. (Note that radio quiet has always meant radio weak, not completely radio silent). Strittmatter et al. (1980) discussed the radio observations of 70 spectroscopically confirmed QSOs selected from the Michigan Curtis Schmidt surveys (MacAlpine et al. 1977a,b,c) and claimed that the distribution of the logarithmic radio flux densities $\log(S)$ of QSOs is sharply bimodal (that is, has two peaks). This stimulated a controversy that persists to this day. However, Condon et al. (2013) recently pointed out that this claim resulted from a mathematical error and is not valid.

More sensitive 5 GHz VLA observations with an rms noise $\sigma \approx 65 \mu\text{Jy beam}^{-1}$ allowed

Kellermann et al. (1989) to detect 82% of the relatively bright ($B \lesssim 16$) *bona fide* QSOs with $M_B < -23$ (old cosmology; $M_B < -22.2$ today) in the Schmidt & Green (1983) Bright Quasar Survey (BQS). They reached a radio/optical flux-density ratio $R = 0.1$ and argued that the distributions of observed $\log(S)$ and $\log(R)$ appeared to be bimodal. Schmidt (1970) preferred R rather than S because it is nearly distance-independent. Also, if the radio and optical luminosities of QSOs are correlated, the distribution of $\log(R)$ should be more narrow than the distribution of $\log(S)$, making it a more efficient discriminator between RLQs and RQQs. The Kellermann et al. (1989) VLA observations of bright QSOs had sufficient sensitivity to divide most of them into an RQQ population defined by $R < 10$ and an RLQ population defined by $R > 10$, with few QSOs falling in the $1 < R < 10$ gap. Goldschmidt et al. (1992) and Miller et al. (1993) noted that large errors in the magnitudes, positions, and redshifts of BQS objects resulted in substantial bias and incompleteness in the BQS, raising questions about the conclusions of Kellermann et al. (1989). Even so, several subsequent radio observations and analyses of other QSO samples appear to support their two-population description (Miller et al. 1990; Stocke et al. 1992; Visnovsky et al. 1992; Goldschmidt et al. 1999; Xu et al. 1999; Ivezić et al. 2002, 2004; Jiang et al. 2007).

However, the claim of two distinct populations was further challenged by a number of other authors who found continuous distributions of $\log(S)$ or $\log(R)$ with no clear gap separating RLQs from RQQs. Using 1.4 GHz radio data from the FIRST survey, Becker et al. (1995); White et al. (2000); Lacy et al. (2001); Cirasuolo et al. (2003a,b); Wals et al. (2005); Rafter et al. (2009); Singal et al. (2011); Bonchi et al. (2013) all reported no evidence for two separate populations, although these conclusions were all based on samples defined by radio surveys, which are highly biased toward the radio-loud population. Moreover, with a 1 mJy beam^{-1} catalog limit, FIRST cannot detect RQQs individually, so White et al. (2007) lowered their noise limit by stacking over 40,000 FIRST images of SDSS QSOs. Unfortunately, the resulting mean flux density is dominated by the very small number of sources just below the FIRST catalog limit (Condon et al. 2013). Cirasuolo et al. (2003a,b) argued that the apparent bimodality claimed by others is the result of bias related to the strong dependence of radio on optical luminosity, but this argument has been refuted by Ivezić et al. (2004).

Using their 20 GHz radio data, Mahony et al. (2012) found no evidence for a separate population of RLQs and RQQs in a sample of 874 X-ray selected quasars, but their X-ray selection biases the sample toward blazars and the 20 GHz ATCA observations barely reach down into the RQQ population.

Terlevich and colleagues (Terlevich et al. 1987; Terlevich 1992; Terlevich et al. 1992) were the first to propose that nearly all QSO emission (radio, optical continuum, and even

the broad emission lines) is powered by starbursts rather than by supermassive black holes (SMBHs). For at least a few of their quasars, Kellermann et al. (1994); Blundell et al. (1996); Blundell & Beasley (1998); Barvainis et al. (2005); Ulvestad et al. (2005), and more recently Herrera Ruiz et al. (2016) and Maini et al. (2016), presented evidence for radio structures extending beyond the host galaxy of stars, radio components with very high surface brightnesses, variability, or apparent superluminal motion, all of which are characteristic of radio emission driven by a SMBH. However, given that these quasars all lie near the Kellermann et al. (1989) $R \sim 10$ boundary between the RQQ and RLQ distributions, they do not provide evidence that RQQs are SMBH-powered.

Sopp & Alexander (1991) noted that most Seyfert galaxies and RQQs obey the far-infrared/radio correlation $\log(L_{\text{FIR}}/L_{\text{Radio}}) \sim -2$ obeyed by nearby star-forming galaxies, while radio-selected galaxies and RLQs have $\log(L_{\text{FIR}}/L_{\text{radio}}) \sim -5$. If far-infrared/radio luminosity ratios are used to *define* the RLQ and RQQ populations, then their sample QSOs have a strongly bimodal distribution in $\log(L_{\text{FIR}}/L_{\text{Radio}})$. Sopp & Alexander (1991) suggested that the RQQs and Seyfert galaxies are spiral galaxies whose radio emission is due to disk star formation, while radio-selected galaxies and RLQs are elliptical galaxies with SMBH-powered radio emission. This scenario suggests that radio sources in RQQs and RLQs are powered *either* by star formation *or* by AGNs, but rarely by both. Thus, like optically selected elliptical galaxies, many QSOs should be “radio silent,” with radio luminosities well below those of normal spiral galaxies.

Kimball et al. (2011) discovered that the distribution of $\log(S_6)$ has few sources with $S_6 \lesssim 20 \mu\text{Jy}$, a distinct “bump” centered on $S_6 \approx 100 \mu\text{Jy}$ and a long, flat tail extending to $S_6 \approx 10^5 \mu\text{Jy}$. This distribution is not bimodal, but neither is it featureless, so it still suggests two populations of QSOs—those in the radio-quiet bump and those in the radio-loud tail. Condon et al. (2013) used NVSS data to statistically find similar 1.4 GHz flux-density distributions in a much larger volume-limited sample of 1313 SDSS QSOs with redshifts $0.2 < z < 0.45$ and for a magnitude-limited sample of 2471 bright ($m_r < +18.5$) high-redshift ($1.8 < z < 2.5$) QSOs.

In narrow redshift ranges, luminosities are strongly correlated with flux densities, so the 6 GHz luminosity functions have similar bumps and tails as the flux density distributions. Spectral luminosities are more fundamental than observed flux densities because they are intrinsic source properties independent of redshift or distance. Kimball et al. (2011) and Condon et al. (2013) suggested (but could not prove) that low-redshift “bump” radio sources with 6 GHz luminosities $L_6 \lesssim 10^{23} \text{ W Hz}^{-1}$ and high-redshift sources with 6 GHz luminosities $L_6 \lesssim 10^{24} \text{ W Hz}^{-1}$ are powered more by star formation in the host galaxy than by the AGN that drives the very luminous optical and infrared emission, while the more luminous “tail”

radio sources are primarily AGN-powered.

In this interpretation, (1) the total radio luminosity of any QSO is the *sum* of its star-formation and AGN-powered contributions, and (2) most QSO host galaxies are currently forming stars. Their median star-formation radio luminosity ranges from $L_6 \approx 10^{22.2} \text{ W Hz}^{-1}$ (about the luminosity of M82) for low-redshift QSOs just brighter than the $M_B = -23$ optical luminosity cutoff to $L_6 \sim 10^{23.5} \text{ W Hz}^{-1}$ (about the luminosity of Arp 220) for the most luminous high-redshift QSOs in the universe ($M_B \sim -28$). The relevant measure of radio loudness is neither the radio flux density S nor the radio–optical flux density ratio R ; it is the radio spectral luminosity L_ν . The boundary separating RLQs from RQQs is not an arbitrary flux density or radio–optical flux density ratio; it is the radio spectral luminosity above which the AGN component usually dominates and below which the star-forming galaxy component contributes significantly. This boundary ranges from $L_6 \sim 10^{23} \text{ W Hz}$ for the least luminous *bona fide* QSOs ($M_B \lesssim -23$) found at low redshifts to $L_6 \sim 10^{24}$ for the most luminous QSOs ($M_B \sim -28$) usually found at higher redshifts. The radio luminosity function of the AGN-powered sources alone is so broad and flat that starbursts contribute more than AGNs to the total radio luminosities of most QSOs. If most RQQs are in star-forming galaxies, not just “red and dead” elliptical galaxies, the typical “radio quiet” QSO should have a total radio luminosity slightly higher than that of its host galaxy alone, and there should be almost no “radio silent” QSOs. Consequently, there is a “bump” in the *total* radio luminosity function of QSOs, and that bump peaks just above the typical luminosity of the star-forming component (Kimball et al. 2011).

Although some QSOs have intermediate levels of luminosity or R , there is no evidence for a separate class of radio-intermediate quasars whose radio emission is driven primarily by an SMBH, as proposed by Falcke et al. (1996). Rather, as described above, we believe that the radio emission from quasars with $L_{1.4} \sim 10^{24} \text{ W Hz}^{-1}$ is due to a mixture of AGN and star forming activity.

Using sub-mJy sources selected from a radio survey of the Chandra Deep Field (Kellermann et al. 2008; Miller et al. 2008, 2013), Padovani et al. (2011, 2014, 2015) have noted that the radio emission from radio-quiet AGNs is also driven by a mixture of SMBHs and star formation, and they derived separate evolving luminosity functions for these two populations. We note, however, that few of the AGNs identified from these sub-mJy radio surveys are *bona fide* QSOs with $M_B < -23$.

Although half a century has passed since the recognition of RQQs, there is still no consensus whether the RLQs represent a separate population of QSOs, or whether they are simply the high luminosity tail of an essentially continuous radio luminosity distribution. Moreover, if RLQs are indeed a separate population, why are only a small fraction of QSOs

strong radio sources? A number of possibilities have been discussed including:

Stellar or Black Hole Mass, Accretion Rate, or Black Hole Spin (e.g., Dunlop et al. 2003; Best et al. 2005; Sikora et al. 2007; Gopal-Krishna et al. 2008; Best & Heckman 2012). Wilson & Colbert (1995) proposed that the main difference between RLQs and RQQs is associated with black hole spin. Black holes are spun up by recent galaxy mergers, and the radio jets of RLQs extract their energy from rapidly spinning black holes. However, there is no evidence for black-hole spin powering of jets in X-ray binaries (Fender et al. 2010), and the role of BH spin in powering quasar radio jets remains uncertain (Heckman & Best 2014).

Intermittent Activity: The radio emission from quasars varies with characteristic times scales of months to years. Typically, the flux density varies by considerably less than an order of magnitude. Longer-term periods of more enhanced brightness would be required to explain the apparent two populations of RLQs and RQQs, and for the extended radio-loud sources, as suggested by the apparent double-double quasars (e.g., Jamrozy et al. 2009; Nandi et al. 2014), time scales of at least 10^5 to 10^6 years would be needed. However, Barvainis et al. (2005) report that RLQs and RQQs show similar variability on time scales of months, and they suggest that in both classes of QSOs, the radio emission is “intimately associated with the active nucleus.”

Absorption: Both synchrotron self absorption and free-free absorption are known to be important in RLQs. Possibly absorption could suppress most of the radio emission and give rise to an apparently radio-quiet population. However, if this were the case we would expect the division between RQQs and RLQs to be much stronger at lower frequencies, and there is no evidence for this (e.g., Mahony et al. 2012).

Host Galaxy Properties: Dunlop et al. (1993); Best & Heckman (2012); Jahnke et al. (2004); Floyd et al. (2013); Falomo et al. (2014) and others have investigated the host galaxies of QSOs and found a mixture of early and late type galaxies, although Dunlop et al. (2003) report that for QSOs with $M_i < -23.5$ (for $H_0 = 50 \text{ km s}^{-1} \text{ Mpc}^{-1}$, or $M_i < -22.7$ for $H_0 = 70 \text{ km s}^{-1} \text{ Mpc}^{-1}$) “the hosts of both RLQs and RQQs are virtually all massive ellipticals.” Thus it appears that the radio loudness of *bona fide* QSOs is not determined by host galaxy morphology.

Relativistic Doppler Beaming: Almost all of the most luminous RLQs exhibit superluminal motion apparently reflecting relativistic Doppler beaming (e.g., Lister et al. 2009). As first suggested by Scheuer & Readhead (1979), it is natural to try to interpret RLQs as the subset of isotropically oriented QSOs whose relativistic beams are aligned close to our line of sight and so have relativistically boosted radio flux densities. However, as discussed in Section 5.2, there are several problems with this apparently attractive interpretation.

3. VLA Observations of Low-redshift QSOs in a Volume-limited Sample

In order to avoid the pitfalls encountered by earlier radio studies of QSOs, as reported by Kimball et al. (2011), we selected a complete sample of QSOs satisfying all of the following:

- (1) SDSS colors well outside the stellar locus in the $(u - g)$, $(g - r)$, $(r - i)$ color cube (Richards et al. 2002). SDSS objects were targeted for spectroscopic follow-up by more than one algorithm. To avoid any bias toward QSO candidates favored for spectroscopic confirmation because they were detected by the 1.4 GHz FIRST survey (Becker et al. 1995), we considered only those QSOs chosen on the basis of color.
- (2) At least one broad emission line with $\text{FWHM} > 1000 \text{ km s}^{-1}$ for spectroscopic confirmation of an AGN.
- (3) $M_i < -23$ to exclude Seyfert nuclei and other low-luminosity AGNs.
- (4) $0.2 < z < 0.3$. This narrow redshift range minimizes the effects of evolution and the degeneracy between luminosity and redshift. The low maximum redshift $z = 0.3$ ensures that sensitive VLA observations can detect sources with luminosities only a few times that of the Milky Way, $L_6 \sim 10^{21.3} \text{ W Hz}^{-1}$. Combined with the requirement that $M_i < -23$, $z < 0.3$ also implies $m_i < 19$ after correction for extinction according to Schlegel et al. (1998). This is brighter than the SDSS completeness limit for QSO spectroscopy, so our QSO sample is truly volume limited. Our sample QSOs are labeled in the SDSS quasar catalog with the flag “low z ” (Richards et al. 2002), as the SDSS targeting algorithm happens to be particularly efficient for the identification of low-redshift quasars.¹
- (5) The $\Omega \approx 3.6 \text{ sr}$ SDSS area bounded by $90^\circ < \text{R.A.} < 300^\circ$, $b > 30^\circ$ is large enough to yield a statistically useful number $N = 179$ of color-selected QSOs in the Schneider et al. (2010) quasar catalog of the seventh data release of the Sloan Digital Sky Survey (SDSS) (Abazajian et al. 2009). We later found that one QSO, J1107+080, is badly confused by an unrelated strong radio galaxy only $3''$ away in projection but at a much lower redshift (Section 4). As we cannot obtain useful radio data for J1107+080 and have no reason to believe that J1107+080 is intrinsically different from the other sample QSOs, we excluded it and used only the remaining 178 QSOs in the following analysis.

We observed using the VLA C configuration with a central frequency of 6 GHz and a bandwidth of 2 GHz in each of the two circular polarizations. With natural weighting the synthesized beamwidth was $3''.5$ FWHM.

We separated the target QSOs into three groups to optimize the observing time. About one-third had already been detected as radio sources by the FIRST (Becker et al. 1995)

¹<http://classic.sdss.org/dr7/>

and/or the NVSS (Condon et al. 1998) surveys with 1.4 GHz peak flux densities ≥ 1 mJy per $5''$ beam or ≥ 2.4 mJy per $45''$ beam, respectively. We re-observed these relatively strong sources for only 90 s at each of two widely different hour angles. All other sources were first observed for 300 s each. Those that were clearly detected with $SNR > 10$ after 300 s were observed for 300 s more at a different hour angle. The fainter remaining sources were re-observed for a total of 30 to 35 minutes, resulting in rms noise levels as low as $\sigma = 6 \mu\text{Jy beam}^{-1}$, which corresponds to a 6 GHz spectral luminosity $L_6 \sim 1.7 \times 10^{21} \sim 10^{21.2} \text{ W Hz}^{-1}$ at $z = 0.3$. Observations of the target quasars were interspersed approximately every 20 minutes with a phase and amplitude calibrator. The flux density scale was determined relative to the source 3C 286 which was observed once each day.

The data were all analyzed within AIPS. After editing for RFI, the data were calibrated, the 16 sub-bands combined, then imaged and cleaned in the AIPS task IMAGR using an 0.2 arcsecond cell size and natural weighting. The images typically covered 200 to 400 arcseconds on a side with resolution of 4 by 5 arcseconds. Where needed to suppress the contamination from a strong source elsewhere in the field, or to enhance the dynamic range of any extended structure, we did one or more rounds of self-calibration. We used the AIPS task JMFIT to measure the peak flux density, angular size, and position of each compact radio component and the AIPS task IMEAN to measure total flux densities of complex extended sources. The systematic position uncertainties are $\lesssim 0''.1$ and $\lesssim 0''.2$ for the compact radio and optical objects, respectively. The rms uncertainty in the radio–optical offset Δ contributed by noise alone is $\sigma_\Delta \sim 1.7\sigma/S_p$. As shown in Figure 1 in all but two cases, there is an apparently unresolved radio source near the QSO position. Although we describe all flux densities as measured at 6 GHz, because of the very large bandwidth used, this is strictly true only if the spectral index is zero. In the more general case for a source with spectral index α (Condon 2015),

$$\nu_u = \left[\left(\frac{1}{\alpha + 1} \right) \left(\frac{\nu_{\max}^{\alpha+1} - \nu_{\min}^{\alpha+1}}{\nu_{\max} - \nu_{\min}} \right) \right]^{1/\alpha}, \quad (\alpha \neq -1) \quad (1)$$

So for a flat bandpass in the range $5 \leq \nu \leq 7$ GHz and $\alpha = -0.7$, the “effective” frequency at which the wideband flux density equals the actual source flux density at 6.00 GHz is 5.952 GHz, and the reported flux densities at 6.00 GHz are too high by 0.56 percent. In the extreme case where $\alpha = -1$, the “effective” frequency is 5.94 GHz, and the reported flux densities too high by 0.94 percent.

Our results are listed in Table 1 as follows:

Column (1): Source name, format SDSS JHHMMSS.SS+DDMMSS.S

Column (2): Seconds of right ascension in the VLA position

Column (3): Arcsec of declination in the VLA position

Column (4): Angular separation Δ between the radio and optical positions (arcsec)

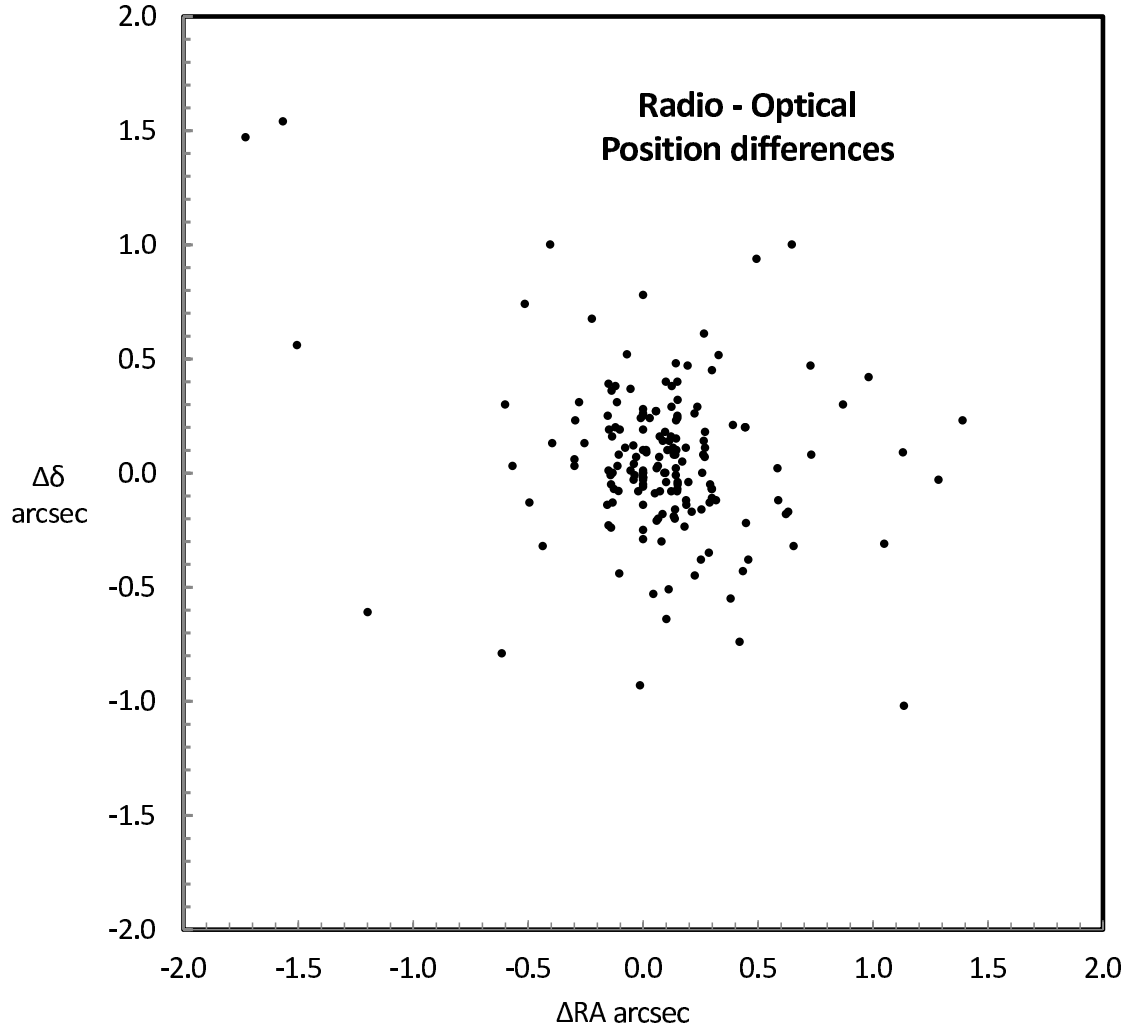


Fig. 1.— Distribution of radio–optical position offsets in arcseconds. Not shown are J0919+143 ($\Delta = 8''.8$, 29 mJy), J1234+644 ($\Delta = 2''.5$, 240 μ Jy), and J1408+630 ($\Delta = 2''.2$, 39 μ Jy).

Column (5): Redshift from the SDSS

Column (6): 6 GHz integrated flux density S (μJy) including any extended structure and its rms error calculated as the quadratic sum of the statistical error and a 3 percent uncertainty in the calibration

Column (7): 6 GHz peak flux density S_p ($\mu\text{Jy beam}^{-1}$) at $3''.5$ resolution and its rms error calculated as in column 6

Column (8): Ratio of peak to integrated flux density

Column (9): Log of the 6 GHz spectral luminosity in the source frame (W Hz^{-1})

Column (10): Apparent i magnitude from the SDSS catalog

Column (11): Absolute I magnitude

Column (12): Ratio R of radio (6 GHz) to optical (i band) flux density calculated from $S_i = 10^{(9.56-i/2.5)} \mu\text{Jy}$

Table 1. Results

(1) QSO Name SDSS	(2) VLA RA (s)	(3) VLA Dec (")	(4) Δ (")	(5) z	(6) S (μ Jy)	(7) S_p (μ Jy beam $^{-1}$)	(8) S_p/S	(9) $\log(L)$ (W Hz $^{-1}$)	(10) i (mag)	(11) I (mag)	(12) R
J075403.60+481428.0	03.617	28.05	0.18	0.276	2631 ± 84.8	2631 ± 84.8	1.000	23.76	17.148	-23.06	5.24
J080829.17+440754.1	29.230	55.10	1.19	0.275	61 ± 11.2	61 ± 11.2	1.000	22.12	17.615	-22.58	0.19
J081652.24+425829.4	52.252	29.21	0.23	0.234	232 ± 13.9	232 ± 13.9	1.000	22.54	16.636	-23.21	0.29
J082205.24+455349.1	05.230	49.18	0.13	0.300	222 ± 11.2	222 ± 11.2	1.000	22.77	17.695	-22.69	0.73
J083353.88+422401.8	53.880	01.75	0.05	0.249	209000 ± 6271	209000 ± 6270	1.000	25.56	16.480	-23.50	225

In Figure 2 we plot the integrated 6 GHz flux densities S against the peak flux densities S_p . With one possible exception, we did not find evidence for any extended structure in any member of the radio-quiet population. SDSS J1458+459 is coincident with an unresolved $43\ \mu\text{Jy}$ radio source. A second source having comparable flux density is located about 5 arcseconds to the east and close to a fainter un-cataloged optical feature. It is not clear if the two radio components are both part of SDSS J1458+459 or if the eastern radio feature is an independent source, possibly associated with the un-cataloged optical object, although there is a $\Delta \sim 1$ arcsecond discrepancy between the radio and optical positions of the secondary feature. The other “discrepant” point is the radio source J0919+143, which by virtue of its 29 mJy extended structure is radio loud even though there is only $265\ \mu\text{Jy}$ in its unresolved core.

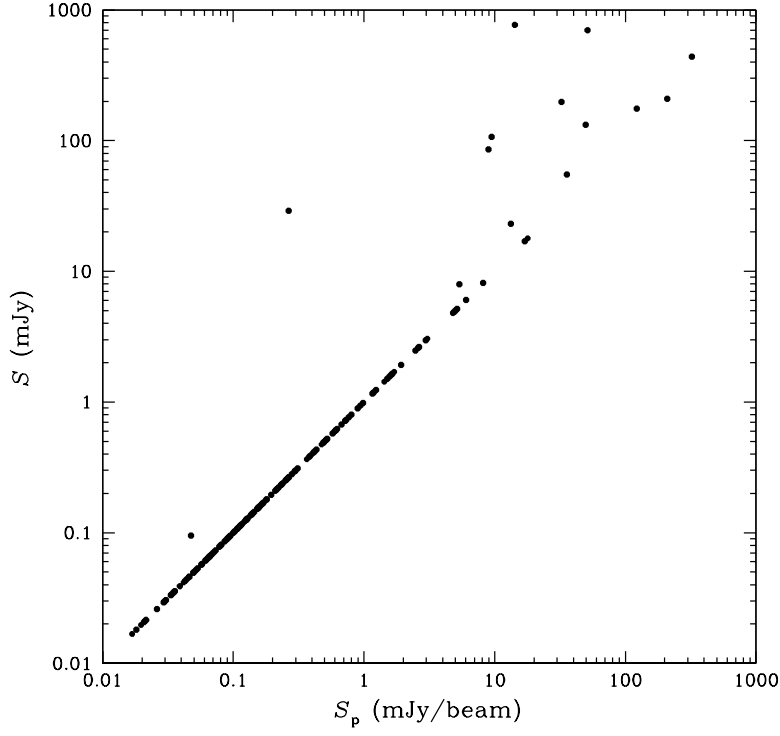


Fig. 2.— Total flux density S (Column 8 of Table 1) vs. peak flux density S_p (Column 9 of Table 1) for the 178 SDSS QSO in our final sample. The values for 1021+190 and 1034+605 are shown at their measured values although they are not considered reliable detections.

Of the 18 SDSS QSOs with unresolved cores stronger than 5 mJy, seven have no observable extended emission. Another source, J1111+483 has a 4.8 mJy feature located about 2 arcmin northwest of the QSO and which is coincident with a magnitude 21.6 red galaxy; so we consider this feature to be unrelated to the SDSS QSO. Five RLQs (J0955+455, J1131+312, J1220+020, J1403+176, and J1527+225) show one-sided extended structure. Seven sources (J0843+206, J0856+599, J0928+604, J0954+213, J1007+128, J1225+249, and J1547+208) show rather symmetric double lobes about equidistant from the optical QSO. One other RLQ, J0919+143 has prominent extended structure but only weak emission near the QSO. In general the extended structure is well resolved, but the outer components of J0843+203 appear remarkably compact, although there are no SDSS counterparts for these compact radio components. The only RQQ showing apparent extended structure (J1458+459) has a companion of about equal flux density located $\approx 5''$ from the QSO that may or may not be associated with the QSO. Figures 3, 4, 5, and 6 show contour plots of the 13 RLQ and 1 RQQ with extended structure.

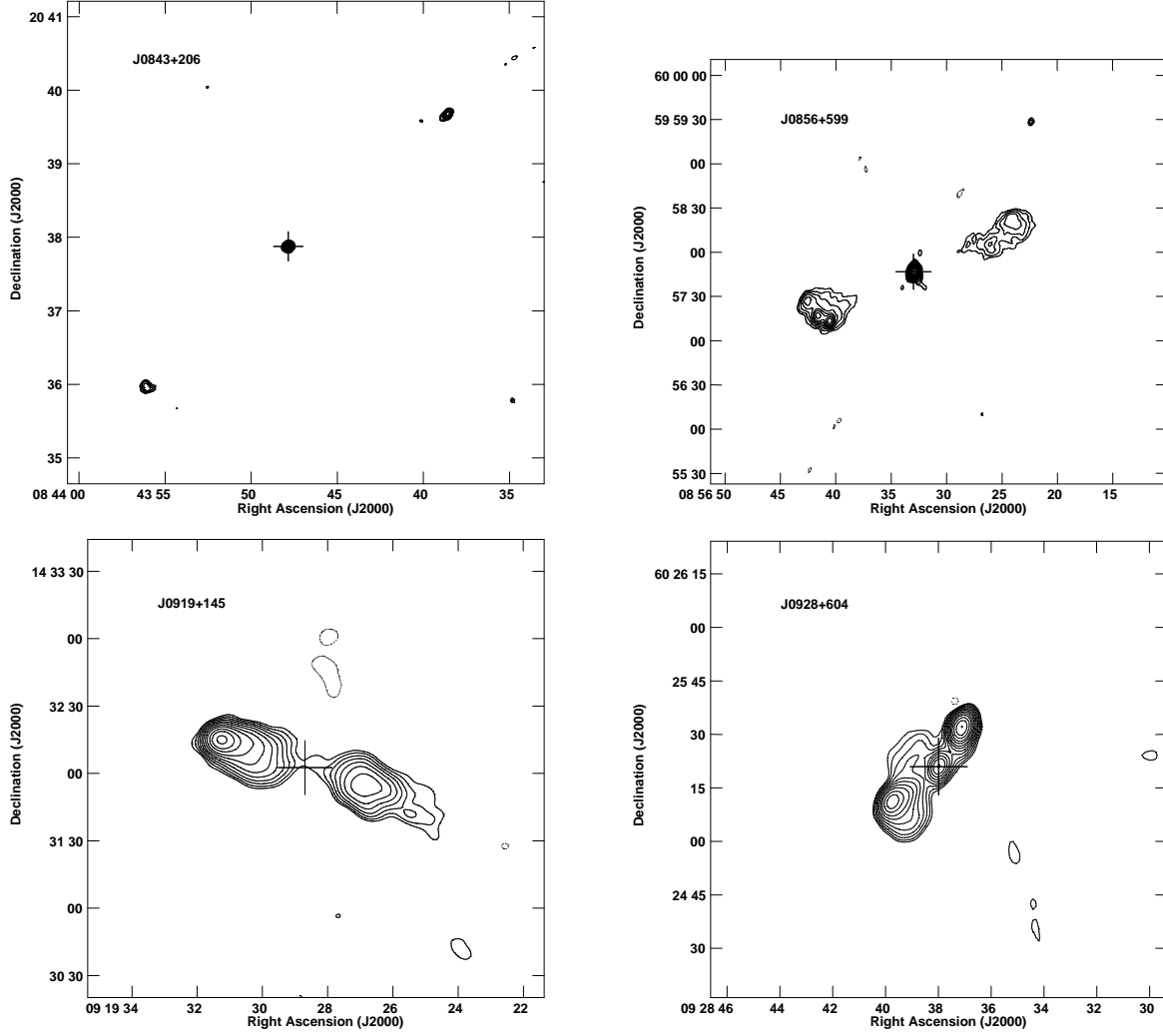


Fig. 3.— Contour maps for the extended radio sources. The cross marks the position of the optical counterpart. Contour intervals are successive factors of $2^{1/2}$ above the lowest contour level, which is $100 \mu\text{Jy beam}^{-1}$ for J0843+206, $200 \mu\text{Jy beam}^{-1}$ for J0856+599 and J0919+145, and $500 \mu\text{Jy beam}^{-1}$ for J0928+604.

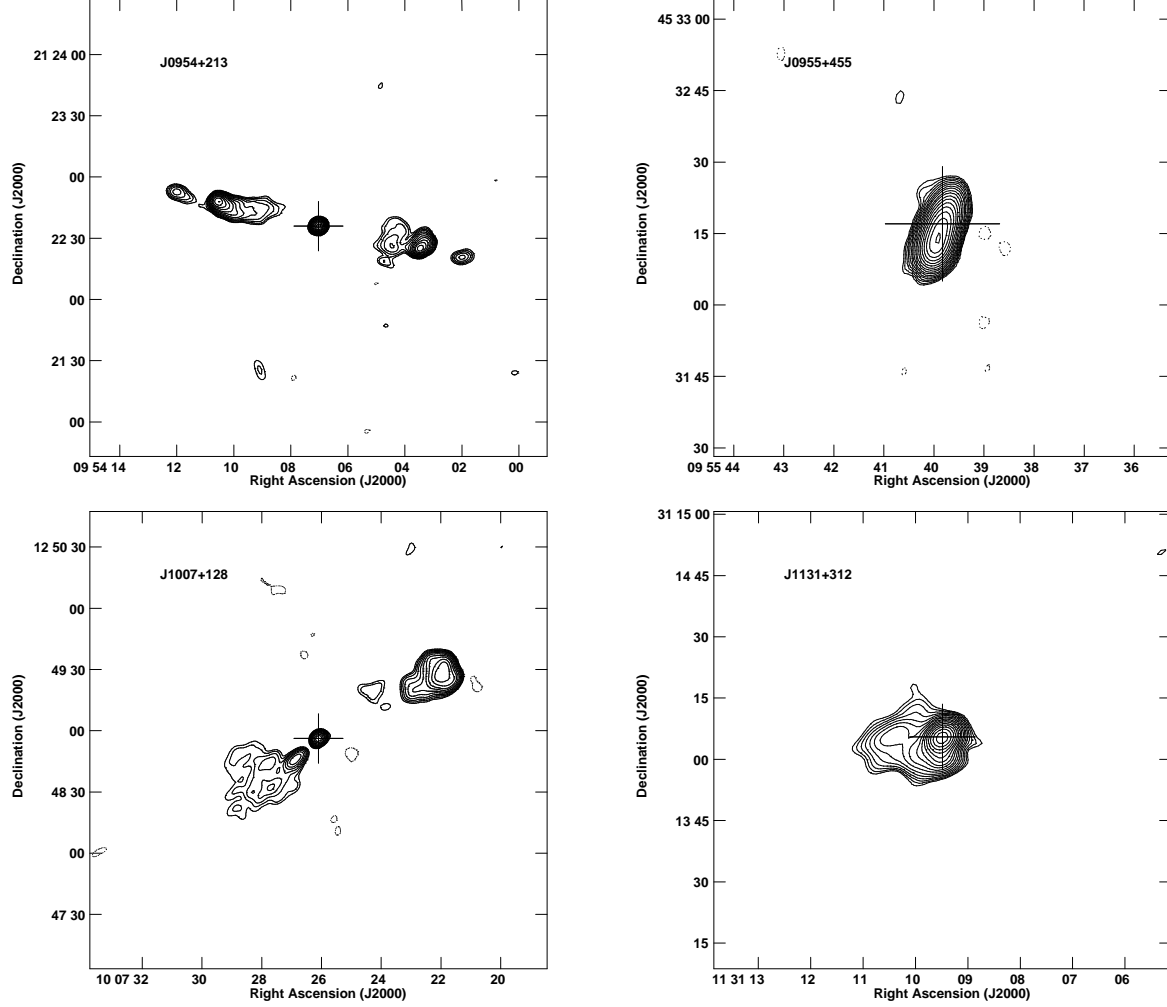


Fig. 4.— Contour maps for the extended radio sources. The cross marks the position of the optical counterpart. Contour intervals are successive factors of $2^{1/2}$ above the lowest contour level, which is $600 \mu\text{Jy beam}^{-1}$ for J0954+213, $50 \mu\text{Jy beam}^{-1}$ for J0955+455, $500 \mu\text{Jy beam}^{-1}$ for J1007+128, and $500 \mu\text{Jy beam}^{-1}$ for J1131+312.

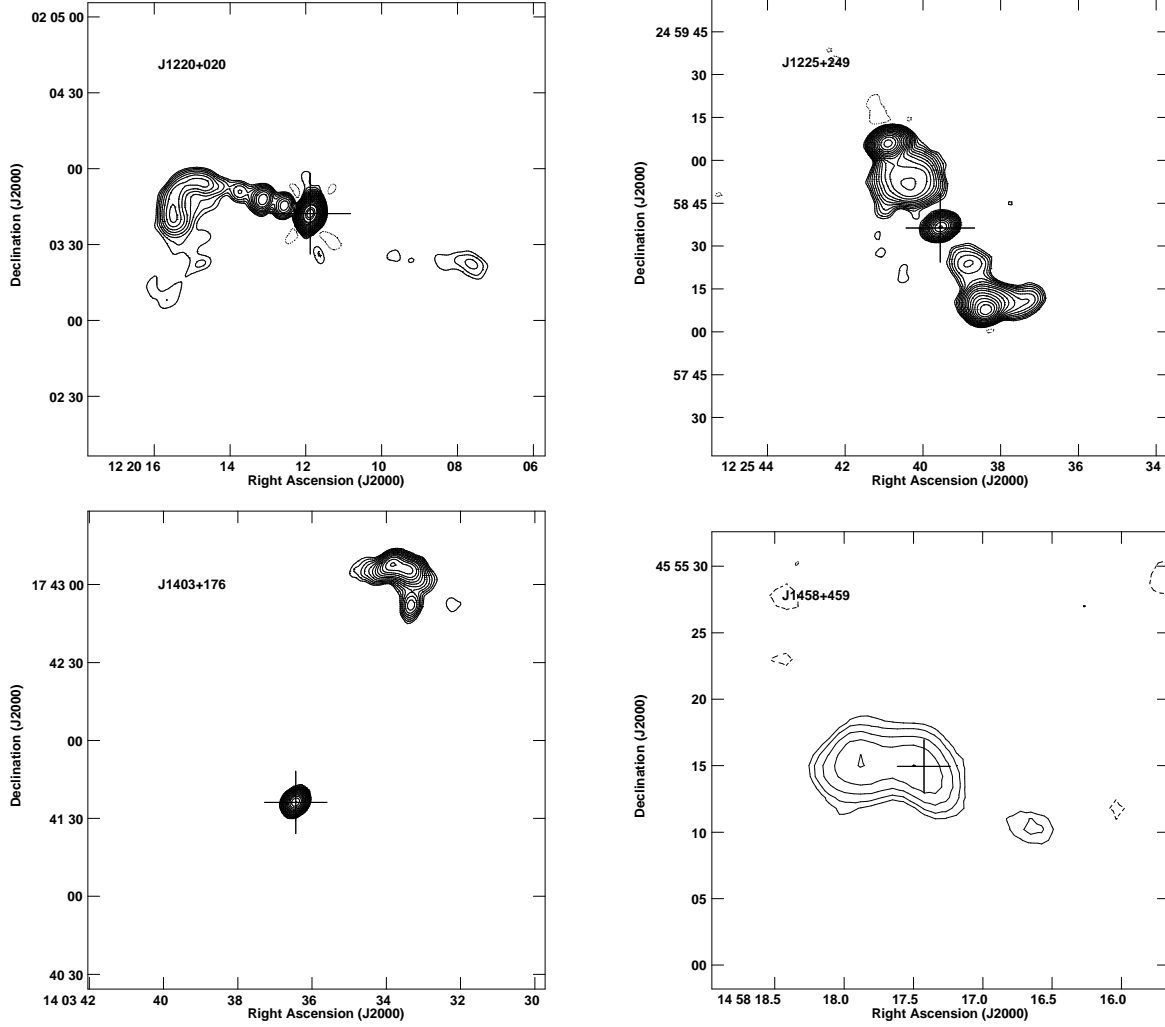


Fig. 5.— Contour maps for the extended radio sources. The cross marks the position of the optical counterpart. Contour intervals are successive factors of $2^{1/2}$ above the lowest contour level, which is $400 \mu\text{Jy beam}^{-1}$ for J1220+020, $100 \mu\text{Jy beam}^{-1}$ for J1225+249, $100 \mu\text{Jy beam}^{-1}$ for J1403+176, and $10 \mu\text{Jy beam}^{-1}$ for J1458+459.

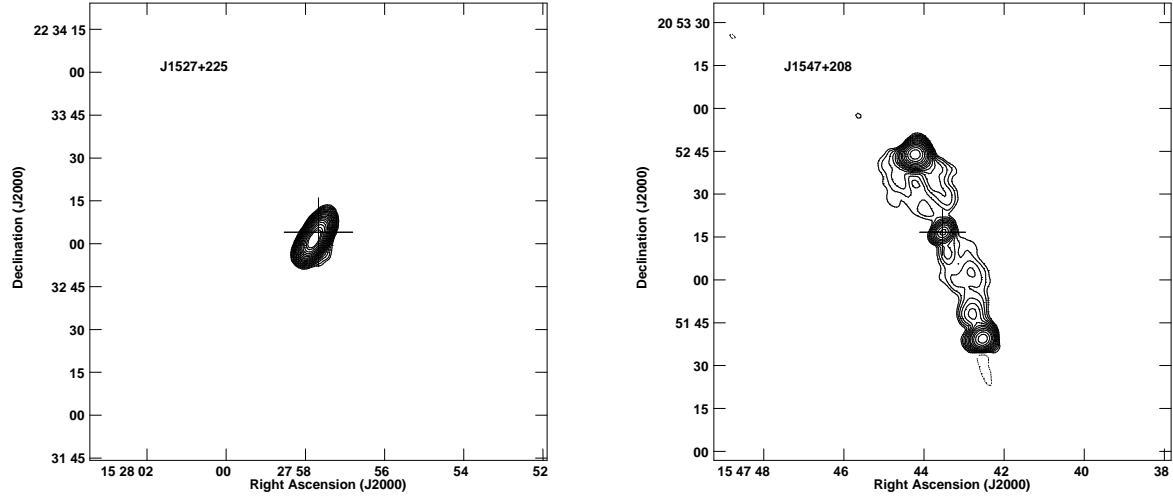


Fig. 6.— Contour maps for the extended radio sources. The cross marks the position of the optical counterpart. Contour intervals are successive factors of $2^{1/2}$ above the lowest contour level, which is $200 \mu\text{Jy beam}^{-1}$ for J152757.67+223304.0 and $2000 \mu\text{Jy beam}^{-1}$ for J154743.53+205216.6.

4. Notes on Individual Sources

Of 179 SDSS quasars observed, we detected radio emission above the 3σ level from all but three. One of them, J1013+020, was probably detected with flux density $S_6 = 21.5 \mu\text{Jy}$ and $SNR = 2.5$ at position offset $\Delta = 1''.1$. The radio image of J1034+600 has poor sensitivity caused by an $S_6 \sim 100 \text{ mJy}$ source only $2'$ from the target QSO, so it was not detected with a 3σ upper limit of $39 \mu\text{Jy}$. J1021+190 was undetected with a 3σ upper limit of $25 \mu\text{Jy}$. Radio sources near J1040+600, J1120+427, J1526+279, and J1544+284 had apparent $3 < SNR < 5$ and offsets $\Delta < 0''.7$, so we consider these to be robust detections. The radio position of J0847+265 differs from the optical position by $\Delta = 1''.1$, but we consider this to be an acceptable offset for a source with $SNR = 3.4$. For J0919+145, the formal position discrepancy is $\Delta = 8''.8$, but J0919+145 is a strong double-lobe source with a component separation of $\sim 90''$ (Figure 3). Its $265 \mu\text{Jy}$ compact core contains only about 1% of the total flux density $S_6 = 29 \text{ mJy}$ and is confused by the strong western lobe, so we do not consider the formal measured radio–optical position difference to be significant.

The radio position of the relatively strong $242 \mu\text{Jy}$ source J1234+644 differs from the SDSS position by $\Delta = 1''.5$. Inspection of the SDSS image reveals a nebulosity surrounding the QSO which may be the QSO host galaxy. Superimposed at the approximate position of the radio source is a condensation which may be part of the host galaxy or possibly a faint foreground galaxy.

The strong ($S_6 = 4.9 \text{ mJy}$) radio source J1107+080 is offset from the QSO position by $\Delta = 3''.05$ and coincides ($\Delta < 0''.2$) with an unrelated $i = 15.1$ galaxy at redshift $z = 0.0734$. The angular separation is comparable with our HPBW, so we cannot make a meaningful measurement of the flux density of the QSO. Therefore we removed this source from our final sample, which reduces it from 179 to 178 QSOs.

We consider all but J1034+605 and J1021+190 to be robust radio detections of radio emission from SDSS quasars. Even if one of the low- SNR detections is not real, the corresponding SDSS QSO is still radio quiet, with maximum flux density well below the $S_6 \approx 100 \mu\text{Jy}$ peak of the radio-quiet distribution, and our conclusions are unchanged.

5. Two QSO Populations

In Figure 7 we show the logarithmic distributions of measured flux densities S_6 , the ratios R of radio (6 GHz) to optical (i mag) flux densities, and the 6 GHz spectral luminosities L_6 for all 178 sources remaining in our SDSS sample. Figure 8 shows the same distributions based on peak flux densities in the $3''.5$ beams coincident with the QSOs.

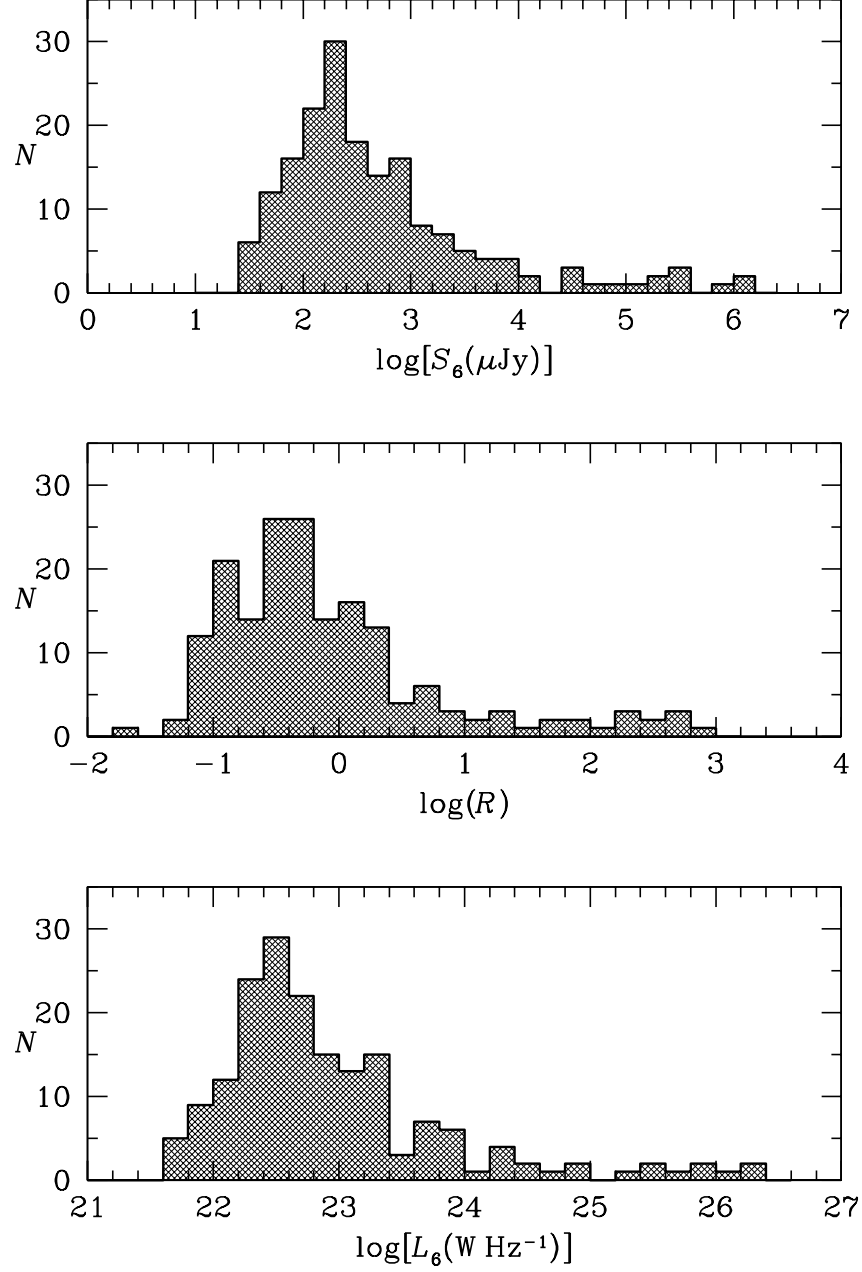


Fig. 7.— Distributions of the radio flux densities, radio/optical flux-density ratios, and radio luminosities from Table 1 columns 6, 12, and 9, respectively. Quasars SDSS J1021+190 and SDSS J1034+608 are plotted at their observed values although they are only marginal detections.

In each of these distributions, we clearly see the presence of two populations as reported earlier by Kimball et al. (2011) and Condon et al. (2013). One has 6 GHz spectral luminosities $L_6 \lesssim 10^{23} \text{ W Hz}^{-1}$. We suggest that the radio emission from these RQQs is the result of active star formation in the host galaxies, and the other more luminous but much smaller population is probably directly related to the central engine associated with the SMBH which powers the optical luminosity. We note that the distributions in Figures 7 and 8 are very similar, so the radio-loud population cannot result from the extended emission alone.

We also recalculated the 6 GHz QSO luminosity function in the redshift range $0.2 < z < 0.3$ using our new flux densities and upper limits. It is shown in Figure 9 and is similar to Figure 2 in Kimball et al. (2011), the most obvious difference being the tighter upper limit to $\log(\rho_m)$ below $L_6 \sim 10^{21} \text{ W Hz}^{-1}$ because four of the six formerly undetected QSOs were detected in the reprocessed data.

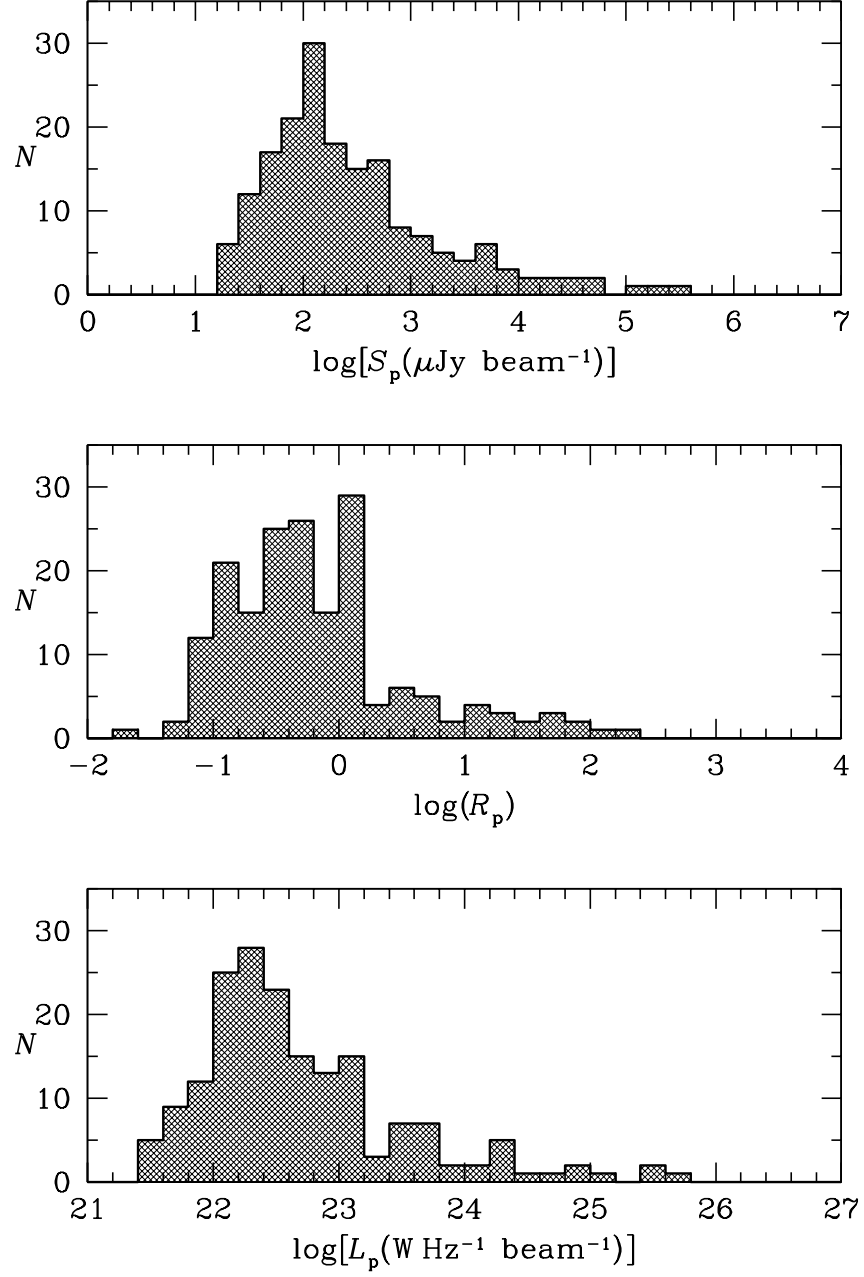


Fig. 8.— Distributions of the radio peak flux densities (column 7 of Table 1), the corresponding peak radio/optical flux-density ratios, and the luminosities calculated from the peak flux densities. Quasars SDSS J1021+190 and SDSS J1034+608 are plotted at their observed values although they are only marginal detections.

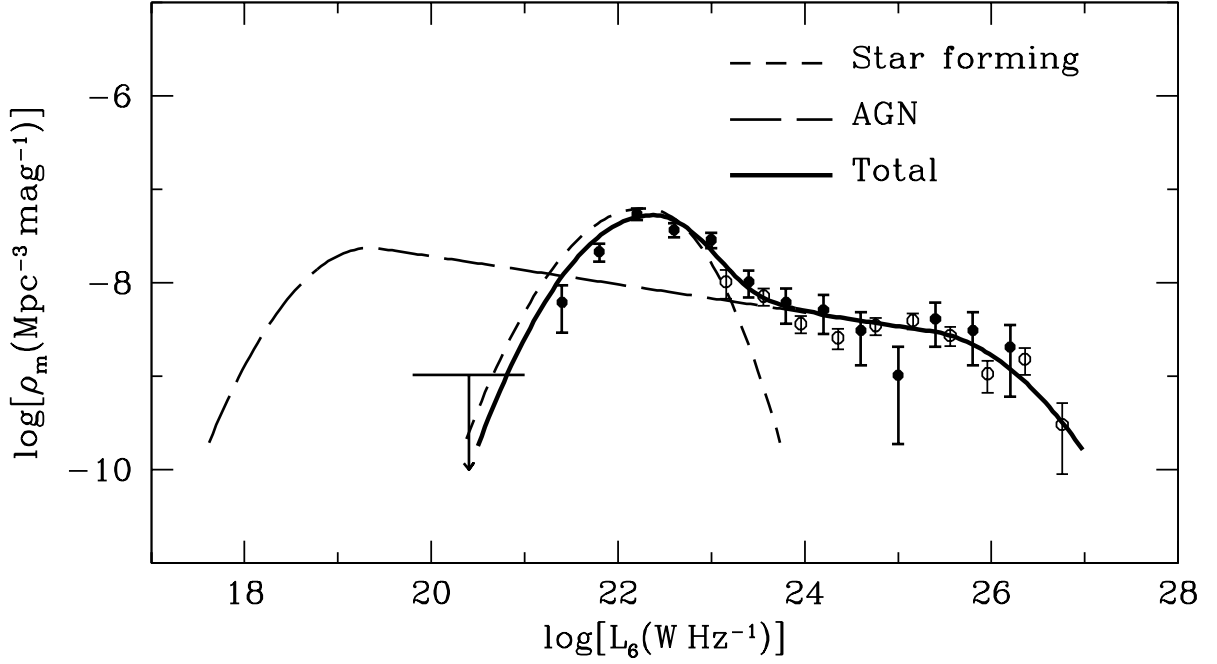


Fig. 9.— The total 6 GHz radio luminosity function of low-redshift QSOs (solid curve) fitted to our 6 GHz VLA data (filled circles and upper limit representing the two undetected sources) and NVSS (Condon et al. 1998) data converted from 1.4 GHz to 6 GHz (Condon et al. 2013) using $\alpha = -0.7$ (open circles) can be decomposed into component luminosity functions contributed by their star-forming host galaxies (short dashed curve) and their AGNs (long dashed curve). At low luminosities the solid curve lies below the dashed curves because the total radio luminosity of each QSO is greater than that of either component.

5.1. The Radio Quiet QSO Population

The 6 GHz radio luminosity $\log[L_6(\text{W Hz}^{-1})] \approx 22.4$ of the RQQ peak (solid curve in Figure 9) and the median spectral index $\langle\alpha\rangle \sim -0.7$ (Condon et al. 2013) of low-redshift RQQs are characteristic of radio emission by relativistic electrons accelerated in supernova remnants of young stars, and they differ from the flat-spectrum optically thick sources almost exclusively associated with AGN. Our hypothesis that the radio emission from RQQs is primarily due to star formation in the host galaxy and is unrelated to the SMBH (Condon et al. 2013) is supported by Jahnke et al. (2004), who reported evidence for ongoing star formation even in the elliptical host galaxies of QSOs. Radio emission from galaxies with active star formation is tightly correlated with FIR emission and is characterized by the ratio $q \equiv \log(S_{\text{FIR}}/S_{1.4}) \sim 2.3$ or $\log(S_{\text{FIR}}/S_6) \sim 2.7$. The 6 GHz radio luminosity function that we attribute to star formation (short dashed curve in Figure 9) peaks at $\log[L_6(\text{W Hz}^{-1})] \approx 22.3$ and corresponds to a star-formation rate $\dot{M} \sim 20 M_\odot \text{ yr}^{-1}$ (Condon et al. 2013).

We note that the absolute radio luminosities of our RQQs are far below the sensitivity limits of nearly all published QSO studies, which have higher flux-density limits and/or include QSOs with higher redshifts. They are also far below the traditional $\log[L_{8.4}(\text{W Hz}^{-1})] \approx 25$ boundary often used to distinguish RLQs from RQQs (Hooper et al. 1996).

As we do not have FIR data for our SDSS sample, following Sargent et al. (2010), Bonzini et al. (2013), and others, we have looked at the distribution of $Q_{22} \equiv \log(S_{22\mu\text{m}}/S_6)$ (Figure 10) based on Band 4 WISE observations and our 6 GHz VLA data. While Figure 10 does reflect the separation between the radio-loud and radio-quiet populations, we do not see the strong correlation between the $22\mu\text{m}$ and 6 GHz flux densities that is characteristic of radio - FIR comparisons. This is not surprising as the measured $22\mu\text{m}$ flux densities are probably dominated by warm dust heated by the AGN (Polletta et al. 2010) and so are not a clean measure of star-forming activity in QSOs.

In principle, radio emission resulting from star formation may be distinguished from black hole AGN emission by examining the radio spectral index. For the radio loud sample, we have compared our 6 GHz images with the 1.4 GHz FIRST and NVSS images. As is characteristic of radio loud quasars and radio galaxies, our radio loud sample is a mixture of flat spectrum cores and steep spectrum extended structure consistent with an AGN origin, but there is no corresponding data for the RQQs at other wavelengths. Ideally one might determine radio spectra of the RQQs just using our 16 separately calibrated sub-bands which cover the frequency range from 5 to 7 GHz. However, as shown by Condon (2015) (eqn. 52), the uncertainty in spectral index calculated in this way is $\sim 10/\text{SNR}$. As seen from figure 7, the typical RQQ has a flux density ~ 100 microJy, where the SNR is about 15. Thus for

the typical RQQ the rms uncertainty in the spectral index would be ~ 1 , or not very useful to discriminate between a star formation or AGN origin.

Recently Zakamska & Greene (2014) and Zakamska et al. (2016) have proposed that the radio emission from many RQQs is synchrotron radiation from relativistic electrons that are accelerated by moving shocks in organized quasar outflows, rather than by star formation. Their proposal was motivated by their observed correlation between radio luminosity and outflow velocities measured from [OIII] $\lambda 5000$ Å emission-line blueshifts in a sample of 568 obscured luminous Type II quasars in the SDSS. However, 386 of the 568 quasars were detected with $S_{1.4} \gtrsim 1$ mJy by FIRST (Becker et al. 1995). By our criterion, this is a sample dominated by radio-selected quasars, not optically selected QSOs. Their median spectral luminosity is $\nu L_\nu = 10^{40}$ erg s $^{-1}$ at $\nu = 1.4$ GHz, or $L_6 \sim 3 \times 10^{23}$ W Hz $^{-1}$ for sources with $\alpha = -0.7$. This is well above the radio luminosities of sources that we suggest are powered by star formation in the host galaxies of low-redshift QSOs (Figure 9), and it would indicate an “astonishing” $\dot{M} \sim 400 M_\odot$ yr $^{-1}$ star-formation rate (Zakamska & Greene 2014). We agree that the radio emission from these quasars is not starburst-powered, but their quasar population does not overlap our RQQ population.

Herrera Ruiz et al. (2016) and Maini et al. (2016) have detected milliarcsecond structure in 5 RQQs, which they argue is evidence for an AGN driven basis for radio emission in RQQs. Their radio sources have a 1.4 GHz luminosity greater than $\sim L_{1.4} = 10^{24}$ W Hz $^{-1}$, the value that is characteristic of RQQs at redshifts ~ 1.5 (Condon et al. 2013). However, we do not exclude the possibility that there is a mixture of AGN and star forming activity that contributes to the high end of the RQQ luminosity function.

White et al. (2015) found a “bump” peaking near $S_{1.4} = 100$ μ Jy in the normalized QSO count $S^2n(S)$ contributed by 74 faint ($18.4 \leq K_S \leq 22.4$ and $M_i \leq -22$) higher-redshift ($0.7 \lesssim z \lesssim 2.8$) VIDEO QSOs. They concluded that this radio emission is predominantly powered by accretion onto SMBHs. Again, the typical radio luminosity in this bump is so high that we do not expect that it can be explained by star formation in low-luminosity QSOs. Our criterion that RQQs have radio spectral luminosities low enough to be explained by star formation ($L_6 \lesssim 10^{23}$ W Hz $^{-1}$) excludes most QSOs that have been called RQQs in the literature.

5.2. The Radio Loud QSO Population

Thirteen RLQs show extended radio structures, all but perhaps two of which are spread over some tens of arcsec or ~ 100 kpc, or much larger than the host galaxy of stars. Thus it

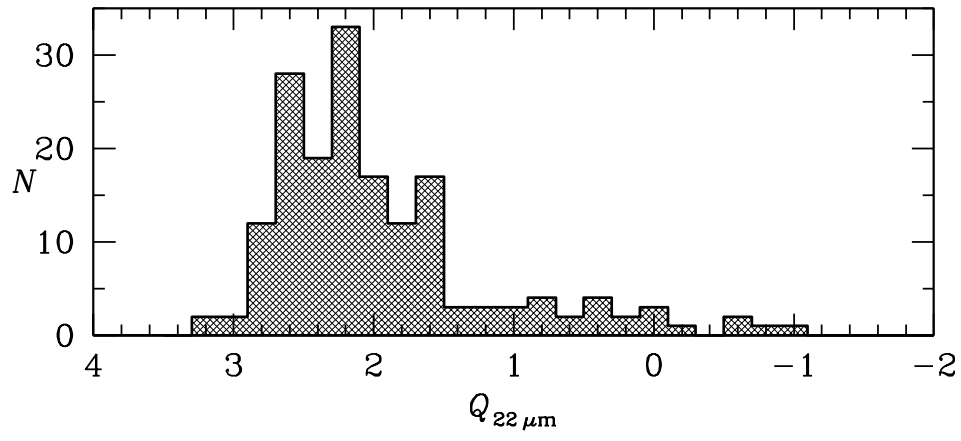


Fig. 10.— Distribution of the ratio of MIR ($\lambda = 22 \mu\text{m}$) to peak radio (6 GHz) flux density. The sources J1021+190 and J1034+608 are shown at their measured values although they are not considered significant detections.

is clear that at least this large scale structure is due to the AGN and can not, as suggested by Terlivich and collaborators, be due to star formation.

Following the widespread recognition of relativistic beaming as the cause of apparent superluminal motion and rapid flux density variability in RLQs, Scheuer & Readhead (1979) made the elegant suggestion that RLQs are just the subset of quasars whose relativistic beams are oriented nearly along the line of sight. Previous radio observations of optically selected QSO samples appeared inconsistent with this simple beaming interpretation. However, the limited sensitivity of these early observations combined with poorly defined QSO selection criteria, use of inappropriate statistics, and differing criteria for separating RLQs from RQQs led to quantitative disagreements with the (Scheuer & Readhead 1979) model. Specifically, it appeared that too many optically selected QSOs appeared radio loud and that the observed detection rate as a function of decreasing flux density was not consistent with simple beaming models.

In view of recent improved observational studies and our increased understanding of relativistic beaming (e.g., Cohen et al. 2007; Lister et al. 2009; Homan et al. 2015), we decided to revisit relativistic beaming models to see if the observed radio-loud / radio-quiet dichotomy for the parsec-scale emission can be explained simply by orientation effects. Following Scheuer & Readhead (1979), in Appendix A we derive the expected radio source count for a population of randomly oriented relativistic jets assuming that the optical emission is unbeamed. As shown by Equation A17, the differential number $n(S) dS$ of detected radio sources between S and $S + dS$ follows a simple power law $n(S) \propto S^\zeta$ whose exponent ζ depends only slightly on the spectral index and geometry of the relativistic beam. For realistic values of spectral index and geometry $-2 < \zeta < -5/4$, so the number of detected radio sources is expected to increase moderately with decreasing flux density.

Considering only the compact components (Column 9 of Table 1) of the radio loud sources alone, we found a best fitting (Crawford et al. 1970) power law index of -1.7 ± 0.2 for the differential source count based on the 18 SDSS sources stronger than 5 mJy. This is marginally steeper than expected from beaming models with flat ($\alpha \sim 0$) spectra which are characteristic of compact blazars. However, our sample is small, and due to the small redshift and corresponding small volume of our SDSS sample, the radio luminosities are low compared with the more powerful, but more rare RLQs, so we would not expect beaming to be very strong in these sources.

Using 1.4 GHz NVSS data for 163 SDSS QSOs stronger than 2.4 mJy and in the redshift range $0.2 < z < 0.45$, Condon et al. (2013) reported $\zeta = -1.20 \pm 0.02$, which is consistent with beaming models. For a sample of 191 more luminous optically selected quasars in the flux-density range $2.4 < S \text{ (mJy)} < 1000$, and redshift range $1.8 < z < 2.5$, Condon et al.

(2013) determined $\zeta = -1.01 \pm 0.02$, which is too large; that is, the observed source count is too “flat”, increasing too slowly as the flux density decreases. The 3σ lower limit $\zeta > -1.07$ is consistent with Equation A17 only for unreasonably steep spectral indices $\alpha \lesssim -10$. In each case, the quoted uncertainties refer to the statistical uncertainty only. Complications such as oblique shocks, a range of intrinsic luminosities or component velocities, contamination by unbeamed lobe emission, etc. only make it harder for beaming to match the data.

Another early objection to the beaming model arose because of the unexpected large fraction of optically selected QSOs that appeared to be radio loud. Because the radiation is beamed into a solid angle $\sim 1/\gamma^2$, with typical observed values $\gamma \sim 10$, it was argued that less than 1 percent of optically (randomly oriented) QSO should appear radio loud, whereas most investigations found 10 to 15 percent to be radio loud. However, in estimating the fraction of optically selected QSOs expected to be radio loud QSOs, the assumption of typical Lorentz factors ~ 10 may not be appropriate. Although samples of radio selected blazars may have typical Lorentz factors ~ 10 , as shown by Lister & Marscher (1997) and Lister et al. (2009), the corresponding much larger parent population is dominated by sources with smaller Lorentz factors and corresponding larger beaming angles. Furthermore, the number flux density distribution predicted from beaming models assumes a simple model with a straight and an infinitely thin jet with a pattern speed equal to the particle speed. However, none of these simplifying assumptions are precisely met in practice (Vermeulen 1995; Lister et al. 2009; Homan et al. 2015), particularly the assumption of straight jets without bends. Also, we note that if the optical emission is also beamed, then even optically selected QSOs will be favorably oriented along the line of sight. Finally, in the so called unified models, an obscuring torus may block optical and IR radiation for those QSOs which are oriented close to the plane of the sky, so that even without consideration of optical beaming, the orientation of even optically selected QSOs may be biased to favor orientations close to the line of sight (Barthel 1989).

The extended radio emission seen in more than half of our RLQs also represents a clear challenge to the Scheuer & Readhead (1979) relativistic beaming interpretation of the radio-loud / radio-quiet dichotomy. The five RLQs with asymmetric large-scale structure might be accommodated within modest relativistic beaming models, and indeed such an interpretation is supported by the facts that parsec and kiloparsec scale structures of RLQs are generally oriented in the same direction (Kellermann & Pauliny-Toth 1981; Barthel 1989) and that RLQs with kiloparsec-scale structures tend to have somewhat slower measured superluminal velocities in the corresponding parsec-scale structures (Zensus 1997). However, the nearly half of the RLQs with two-sided extended structure implies little or no differential Doppler boosting suggesting that the orientation of Doppler boosting is not the major effect separating the RLQs from the RQs.

As shown in Figure 8 the distributions of peak (parsec scale) flux densities S_p , radio-optical ratios R , and radio luminosities L_6 are all similar to the corresponding distributions derived from total flux densities. Thus it is clearly not the extended emission alone that distinguishes RLQs from RQQs.

6. Summary

We have reprocessed the VLA observations of a sample of SDSS QSOs discussed in Kimball et al. (2011), and generated a catalog of radio sources associated with each QSO. We confirm the idea that QSO radio emission comes in two flavors, as indeed some have argued for decades, and strengthen the suggestion made in Kimball et al. (2011) that the emission in most luminous objects is associated with SMBHs, while the emission in the less luminous objects that dominate the sample is associated with the formation of stars in the host galaxies. We detected radio emission at 6 GHz from all but two of the 178 color-selected SDSS QSOs contained in our volume-limited sample of QSOs more luminous than $M_i = -23$ and with redshifts $0.2 < z < 0.3$.

About 20% of these QSOs have 6 GHz source-frame luminosities $L_6 \gtrsim 10^{23} \text{ W Hz}^{-1}$, high enough that SMBHs are probably needed to power most of their radio emission; we call these radio-loud QSOs (RLQs). The RLQ radio luminosity function is flat and featureless. Extrapolating it to lower luminosities indicates that the radio power from many SMBHs should be much less than $L_6 \sim 10^{21} \text{ W Hz}^{-1}$. Radio-quiet QSOs (RQQs) cause a “bump” in the QSO luminosity function spanning $21 \lesssim \log[L_6(\text{W Hz}^{-1})] \lesssim 23$, and “radio-silent” QSOs fainter than $L_6 \sim 10^{21} \text{ W Hz}^{-1}$ are actually quite rare, accounting for not more than 1% of all QSOs. We suggest that the RQQ “bump” is evidence for radio emission powered by star formation in QSO host galaxies, and the lack of radio-silent QSOs is evidence that most RQQ host galaxies are forming stars at least as fast as the Milky Way. Thus RLQs and RQQs may represent two separate populations whose radio emission is dominated by distinctly different energy sources. These populations can be distinguished only by very sensitive radio observations of low-redshift QSOs. Nearly all published attempts to distinguish such RLQs from RQQs have not reached the necessary luminosity level, $L_6 \lesssim 10^{21} \text{ W Hz}^{-1}$.

Many of the RLQs show extended structures, most of which are rather symmetrically located about the parent QSO. While relativistic beaming may play a role in the determining the parsec-scale radio flux densities of some QSOs, the presence of RLQs with symmetric extended structures would seem to require that another mechanism as well is important in determining whether or not a QSO becomes radio loud. Moreover, the flux-density distribution of the RLQ population does not seem to be consistent with simple relativistic beaming

models.

After 50 years of studies of QSO radio dichotomy, technology has finally advanced enough to provide clues for the behavior of radio-quiet objects.

The VLA is a facility of the National Radio Astronomy Observatory which is operated by Associated Universities, Inc., under a Cooperative Agreement with the National Science Foundation. Part of this work was done while one of us (AK) was at the CSIRO Astronomy & Space Science Australia Telescope National Facility. We thank Paolo Padovani and the referee for comments and suggestions which have improved the presentation.

Facilities: VLA.

A. Appendix

When a single source approaches an observer with velocity \vec{v} at an angle θ from the line of sight, the observed frequency ν equals the emitted frequency ν' multiplied by the Doppler factor

$$\delta \equiv \frac{\nu}{\nu'} = [\gamma(1 - \beta \cos \theta)]^{-1} = [\gamma(1 - \beta l)]^{-1}, \quad (\text{A1})$$

where $\beta \equiv v/c$, $\gamma \equiv (1 - \beta^2)^{-1/2}$ is the Lorentz factor, and $l \equiv \cos \theta$ is the direction cosine of θ .

For a population of sources with randomly oriented velocities, the probability that \vec{v} will point toward any solid angle Ω is $\Pi(\Omega) = (4\pi)^{-1}$, and the probability distribution of Doppler factors δ can be calculated from $\Pi(\delta) d\delta = |\Pi(\Omega) d\Omega|$.

$$\Pi(\delta) = \frac{1}{4\pi} \left| \frac{d\Omega}{d\delta} \right| = \frac{1}{4\pi} \left| \frac{d\delta}{dl} \frac{dl}{d\Omega} \right|^{-1} \quad (\text{A2})$$

The ring between θ and $\theta + d\theta$ covers solid angle

$$d\Omega = 2\pi \sin \theta d\theta = -2\pi d(\cos \theta) = -2\pi dl \quad (\text{A3})$$

and

$$\frac{d\delta}{dl} = \frac{\gamma\beta}{[\gamma(1 - \beta l)]^2} = \gamma\beta\delta^2 \quad (\text{A4})$$

so

$$\Pi(\delta) = (2\gamma\beta\delta^2)^{-1} \quad (\text{A5})$$

in the range

$$[\gamma(1 + \beta)]^{-1} < \delta < [\gamma(1 - \beta)]^{-1} = \gamma(1 + \beta) \quad (\text{A6})$$

corresponding to the range of angles $0 < \theta < \pi$. In the limit $\beta \rightarrow 1$,

$$(2\gamma)^{-1} < \delta < 2\gamma . \quad (\text{A7})$$

The quantity I_ν/ν^3 , where I_ν is spectral brightness, is Lorentz invariant (Rybicki & Lightman 1979). The observed flux density $S(\nu)$ of a moving source emitting flux density $S'(\nu')$ isotropically in its frame is

$$\frac{S(\nu)}{S'(\nu')} = \left(\frac{\nu}{\nu'}\right)^3 = \delta^3 . \quad (\text{A8})$$

(Rybicki & Lightman 1979). In terms of the spectral index $\alpha \equiv +d \ln S / d \ln \nu$ (positive sign convention), the flux density of a source with a power-law spectrum is

$$S'(\nu') = S'(\nu) \left(\frac{\nu'}{\nu}\right)^\alpha = \delta^{-\alpha} \quad (\text{A9})$$

so

$$S(\nu) = S'(\nu) \delta^{3-\alpha} \quad (\text{A10})$$

Equation A10 applies to a single emitting region, or source component. The observed lifetime τ of a source with proper lifetime τ' is $\tau = \delta^{-1}\tau'$. The time-averaged flux density of a radio source consisting of multiple identical components with the same velocity created at a nearly uniform rate $\gg \tau^{-1}$ (e.g., a radio jet) will be proportional to τ , or $S(\nu) \propto \delta^{2-\alpha}$. To allow for time averaging over a population of source components having finite lifetimes and different Doppler factors, let

$$S(\nu) = S'(\nu) \delta^{p-\alpha} , \quad (\text{A11})$$

where $S'(\nu)$ is the total flux density in the source frame and $p = 2$. Again, for any single component, $p = 3$.

Doppler boosting broadens the flux-density distribution of a population of intrinsically identical sources characterized by the same γ and $S'(\nu) = 1$. The probability distribution of observed flux density is $\Pi(S)dS = |\Pi(\delta)d\delta|$.

$$\Pi(S) = \Pi(\delta) \left| \frac{dS}{d\delta} \right|^{-1} \quad (\text{A12})$$

Differentiating Equation A11 yields

$$\frac{dS}{d\delta} = (p - \alpha)\delta^{p-\alpha-1} \quad (\text{A13})$$

Inserting Equation A5 for isotropically oriented sources gives

$$\Pi(S) = [2\gamma\beta(p - \alpha)\delta^{p-\alpha+1}]^{-1} \quad (\text{A14})$$

In terms of the observed flux density S ,

$$\Pi(S) = [2\gamma\beta(p - \alpha)]^{-1} S^{-\left(\frac{p-\alpha+1}{p-\alpha}\right)} \quad (\text{A15})$$

over the flux-density range $[\gamma(1 + \beta)]^{\alpha-p} < S < [\gamma(1 + \beta)^p - \alpha]$. Equation A15 specifies the flux-density distribution of a population of intrinsically identical and isotropically oriented sources.

For example, consider a population of identical optically selected QSOs and assume that the optical emission is unbeamed, so the QSOs have random orientations. Assume further that each QSO has one radio component with intrinsic flux density $S(\nu) = 1$ moving with Lorentz factor γ . If there are N_0 QSOs per steradian, the differential count $n(S)$ of radio sources per steradian is given by $n(S) = N_0\Pi(S)$ or

$$n(S) = \left[\frac{N_0}{2\gamma\beta(p - \alpha)} \right] S^{\left(\frac{p-\alpha+1}{\alpha-p}\right)} \quad (\text{A16})$$

The quantity in square brackets is independent of S , so $n(S) \propto S^\zeta$ is a power law with slope ζ given by

$$\zeta = \left(\frac{p - \alpha + 1}{\alpha - p} \right). \quad (\text{A17})$$

For any combination of $2 < p < 3$ and $-1 < \alpha < +1$, the *flatest* slope occurs with $\zeta = -5/4$, which occurs for $p = 3$, $\alpha = -1$; the *steepest* slope is $\zeta = -2$, when $p = 2$, $\alpha = +1$.

REFERENCES

- Abazajian, K. N., Adelman-McCarthy, J. K., Agüeros, M. A., et al. 2009, *ApJS*, 182, 543
- Barthel, P. D. 1989, *ApJ*, 336, 606
- Barvainis, R., Lehár, J., Birkinshaw, M., Falcke, H., & Blundell, K. M. 2005, *ApJ*, 618, 108
- Becker, R. H., White, R. L., & Helfand, D. J. 1995, *ApJ*, 450, 559
- Best, P. N., Kauffmann, G., Heckman, T. M., et al. 2005, *MNRAS*, 362, 25
- Best, P. N., & Heckman, T. M. 2012, *MNRAS*, 421, 1569
- Blundell, K. M., Beasley, A. J., Lacy, M., & Garrington, S. T. 1996, *ApJ*, 468, L91
- Blundell, K. M., & Beasley, A. J. 1998, *Bulletin of the American Astronomical Society*, 30, #110.04
- Bonchi, A., La Franca, F., Melini, G., Bongiorno, A., & Fiore, F. 2013, *MNRAS*, 429, 1970
- Bonzini, M., Padovani, P., Mainieri, V., et al. 2013, *MNRAS*, 436, 3759
- Chiu, H.-Y. 1964, *Physics Today*, 17, 21
- Cirasuolo, M., Celotti, A., Magliocchetti, M., & Danese, L. 2003, *MNRAS*, 346, 447
- Cirasuolo, M., Magliocchetti, M., Celotti, A., & Danese, L. 2003, *MNRAS*, 341, 993
- Cohen, M. H., Lister, M. L., Homan, D. C., et al. 2007, *ApJ*, 658, 232
- Condon, J. J., Condon, M. A., Mitchell, K. J., & Usher, P. D. 1980, *ApJ*, 242, 486
- Condon, J. J., Odell, S. L., Puschell, J. J., & Stein, W. A. 1980, *Nature*, 283, 357
- Condon, J. J., Cotton, W. D., Greisen, E. W., et al. 1998, *AJ*, 115, 1693
- Condon, J. J., Kellermann, K. I., Kimball, A. E., Ivezić, Ž., & Perley, R. A. 2013, *ApJ*, 768, 37
- Condon, J. 2015, *arXiv:1502.05616*
- Crawford, D. F., Jauncey, D. L., & Murdoch, H. S. 1970, *ApJ*, 162, 405
- Herrera Ruiz, N., Middelberg, E., Norris, R. P., & Maini, A. 2016, *A&A*, 589, L2
- Dunlop, J. S., Taylor, G. L., Hughes, D. H., & Robson, E. I. 1993, *MNRAS*, 264, 455

- Dunlop, J. S., McLure, R. J., Kukula, M. J., et al. 2003, MNRAS, 340, 1095
- Falcke, H., Sherwood, W., & Patnaik, A. R. 1996, ApJ, 471, 106
- Falomo, R., Bettoni, D., Karhunen, K., Kotilainen, J. K., & Uslenghi, M. 2014, MNRAS, 440, 476
- Floyd, D. J. E., Dunlop, J. S., Kukula, M. J., et al. 2013, MNRAS, 429, 2
- Goldschmidt, P., Miller, L., La Franca, F., & Cristiani, S. 1992, MNRAS, 256, 65P
- Goldschmidt, P., Kukula, M. J., Miller, L., & Dunlop, J. S. 1999, ApJ, 511, 612
- Gopal-Krishna, Mangalam, A., & Wiita, P. J. 2008, ApJ, 680, L13
- Greenstein, J. L. 1963, Nature, 197, 1041
- Greenstein, J. L., & Schmidt, M. 1964, ApJ, 140, 1
- Fanti, C., Fanti, R., Lari, C., et al. 1977, A&A, 61, 487
- Fender, R. P., Gallo, E., & Russell, D. 2010, MNRAS, 406, 1425
- Heckman, T. M., & Best, P. N. 2014, ARA&A, 52, 589
- Herrera Ruiz, N., Middelberg, E., Norris, R. P., & Maini, A. 2016, A&A, 589, L2
- Homan, D. C., Lister, M. L., Kovalev, Y. Y., et al. 2015, ApJ, 798, 134
- Hooper, E. J., Impey, C. D., Foltz, C. B., & Hewett, P. C. 1996, ApJ, 473, 746
- Ivezić, Ž., Menou, K., Knapp, G. R., et al. 2002, AJ, 124, 2364
- Ivezić, Z., Richards, G., Hall, P., et al. 2004, AGN Physics with the Sloan Digital Sky Survey, 311, 347
- Jamrozy, M., Saikia, D. J., & Konar, C. 2009, MNRAS, 399, L141
- Jiang, L., Fan, X., Ivezić, Ž., et al. 2007, ApJ, 656, 680
- Jahnke, K., Kuhlbrodt, B., & Wisotzki, L. 2004, MNRAS, 352, 399
- Katgert, P., Katgert-Merkelijn, J. K., Le Poole, R. S., & van der Laan, H. 1973, A&A, 23, 171
- Kellermann, K. I., & Pauliny-Toth, I. I. K. 1966, Nature, 212, 781

- Kellermann, K. I., & Pauliny-Toth, I. I. K. 1981, *ARA&A*, 19, 373
- Kellermann, K. I., Sramek, R., Schmidt, M., Shaffer, D. B., & Green, R. 1989, *AJ*, 98, 1195
- Kellermann, K. I., Sramek, R. A., Schmidt, M., Green, R. F., & Shaffer, D. B. 1994, *AJ*, 108, 1163
- Kellermann, K. I., Fomalont, E. B., Mainieri, V., et al. 2008, *ApJS*, 179, 71
- Kimball, A. E., Kellermann, K. I., Condon, J. J., Ivezić, Ž., & Perley, R. A. 2011, *ApJ*, 739, L29
- Kinman, T. D. 1965, *ApJ*, 142, 1241
- Lacy, M., Laurent-Muehleisen, S. A., Ridgway, S. E., Becker, R. H., & White, R. L. 2001, *ApJ*, 551, L17
- Lister, M. L., & Marscher, A. P. 1997, *ApJ*, 476, 572
- Lister, M. L., Cohen, M. H., Homan, D. C., et al. 2009, *AJ*, 138, 1874
- Lynds, C. R., & Villere, G. 1965, *ApJ*, 142, 1296
- MacAlpine, G. M., Smith, S. B., & Lewis, D. W. 1977, *ApJS*, 34, 95
- MacAlpine, G. M., Smith, S. B., & Lewis, D. W. 1977, *ApJS*, 35, 197
- MacAlpine, G. M., Lewis, D. W., & Smith, S. B. 1977, *ApJS*, 35, 203
- Mahony, E. K., Sadler, E. M., Croom, S. M., et al. 2012, *ApJ*, 754, 12
- Maini, A., Prandoni, I., Norris, R. P., Giovannini, G., & Spitler, L. R. 2016, *A&A*, 589, L3
- Miller, L., Peacock, J. A., & Mead, A. R. G. 1990, *MNRAS*, 244, 207
- Miller, P., Rawlings, S., & Saunders, R. 1993, *MNRAS*, 263, 425
- Miller, N. A., Fomalont, E. B., Kellermann, K. I., et al. 2008, *ApJS*, 179, 114
- Miller, N. A., Bonzini, M., Fomalont, E. B., et al. 2013, *ApJS*, 205, 13
- Nandi, S., Roy, R., Saikia, D. J., et al. 2014, *ApJ*, 789, 16
- Padovani, P., Miller, N., Kellermann, K. I., et al. 2011, *ApJ*, 740, 20
- Padovani, P., Bonzini, M., Miller, N., et al. 2014, *IAU Symposium*, 304, 79

- Padovani, P., Bonzini, M., Kellermann, K. I., et al. 2015, MNRAS, 452, 1263
- Polletta, M., Maraschi, L., Chiappetti, L., et al. 2010, Accretion and Ejection in AGN: a Global View, 427, 116
- Rafter, S. E., Crenshaw, D. M., & Wiita, P. J. 2009, AJ, 137, 42
- Richards, G. T., Fan, X., Newberg, H. J., et al. 2002, AJ, 123, 2945
- Rybicki, G. B., & Lightman, A. P. 1979, *Radiative Processes in Astrophysics* (New York: Wiley)
- Sandage, A. 1965, ApJ, 141, 1560
- Sargent, M. T., Schinnerer, E., Murphy, E., et al. 2010, ApJ, 714, L190
- Scheuer, P. A. G., & Readhead, A. C. S. 1979, Nature, 277, 182
- Schlegel, D. J., Finkbeiner, D. P., & Davis, M. 1998, ApJ, 500, 525
- Schmidt, M. 1963, Nature, 197, 1040
- Schmidt, M. 1965, ApJ, 141, 1295
- Schmidt, M. 1970, ApJ, 162, 871
- Schmidt, M., & Green, R. F. 1983, ApJ, 269, 352
- Schneider, D. P., Richards, G. T., Hall, P. B., et al. 2010, AJ, 139, 2360
- Shaffer, D., Green, R., & Schmidt, M. 1982, Extragalactic Radio Sources, 97, 367
- Shapiro, I. I., & Weinreb, S. 1966, ApJ, 143, 598
- Sikora, M., Stawarz, L., & Lasota, J.-P. 2007, ApJ, 658, 815
- Singal, J., Petrosian, V., Lawrence, A., & Stawarz, L. 2011, ApJ, 743, 104
- Smith, M. G., & Wright, A. E. 1980, MNRAS, 191, 871
- Sopp, H. M., & Alexander, P. 1991, MNRAS, 251, 14P
- Sramek, R. A., & Weedman, D. W. 1980, ApJ, 238, 435
- Stoeke, J. T., Morris, S. L., Weymann, R. J., & Foltz, C. B. 1992, ApJ, 396, 487

- Strittmatter, P. A., Hill, P., Pauliny-Toth, I. I. K., Steppe, H., & Witzel, A. 1980, *A&A*, 88, L12
- Terlevich, R., Melnick, J., & Moles, M. 1987, *Observational Evidence of Activity in Galaxies*, 121, 499
- Terlevich, R. 1992, *ASPC*, 31, 133
- Terlevich, R., Tenorio-Tagle, G., Franco, J., & Melnick, J. 1992, *MNRAS*, 255, 713
- Ulvestad, J. S., Antonucci, R. R. J., & Barvainis, R. 2005, *ApJ*, 621, 123
- Vermeulen, R. C. 1995, *Proceedings of the National Academy of Science*, 92, 11385
- Visnovsky, K. L., Impey, C. D., Foltz, C. B., et al. 1992, *ApJ*, 391, 560
- Wals, M., Boyle, B. J., Croom, S. M., et al. 2005, *MNRAS*, 360, 453
- White, R. L., Becker, R. H., Gregg, M. D., et al. 2000, *ApJS*, 126, 133
- White, R. L., Helfand, D. J., Becker, R. H., Glikman, E., & de Vries, W. 2007, *ApJ*, 654, 99
- White, S. V., Jarvis, M. J., Häußler, B., & Maddox, N. 2015, *MNRAS*, 448, 2665
- Wilson, A. S., & Colbert, E. J. M. 1995, *ApJ*, 438, 62
- Xu, C., Livio, M., & Baum, S. 1999, *AJ*, 118, 1169
- Zakamska, N. L., & Greene, J. E. 2014, *MNRAS*, 442, 784
- Zakamska, N. L., Lampayan, K., Petric, A., et al. 2016, *MNRAS*, 455, 4191
- Zensus, J. A. 1997, *ARA&A*, 35, 607
- Zwicky, F. 1965, *ApJ*, 142, 1293